

See discussions, stats, and author profiles for this publication at: <https://www.researchgate.net/publication/324004949>

# Forward modeling of thermally activated single-domain magnetic particles applied to First Order Reversal Curves (FORCs)

Article in *Journal of Geophysical Research: Solid Earth* · March 2018

DOI: 10.1002/2018JB015463

CITATIONS

2

READS

97

2 authors:



**Luca Lanci**

Università degli Studi di Urbino "Carlo Bo"

172 PUBLICATIONS 1,751 CITATIONS

[SEE PROFILE](#)



**Dennis V. Kent**

Rutgers University & Lamont-Doherty Earth Observatory of Columbia University

385 PUBLICATIONS 24,569 CITATIONS

[SEE PROFILE](#)

Some of the authors of this publication are also working on these related projects:



Colorado Plateau Coring Project [View project](#)



Viminacium Mammoths [View project](#)

## RESEARCH ARTICLE

10.1002/2018JB015463

## Key Points:

- Numerical model provides a solid base for interpretation of FORC diagrams of SP/SD particles
- Results from thermally activated Stoner-Wohlfarth approach improve previous models based on Preisach theory

## Supporting Information:

- Supporting Information S1
- Data Set S1

## Correspondence to:

L. Lanci,  
luca.lanci@uniurb.it

## Citation:

Lanci, L., & Kent, D. V. (2018). Forward modeling of thermally activated single-domain magnetic particles applied to first-order reversal curves. *Journal of Geophysical Research: Solid Earth*, 123. <https://doi.org/10.1002/2018JB015463>

Received 18 JAN 2018

Accepted 18 MAR 2018

Accepted article online 25 MAR 2018

## Forward Modeling of Thermally Activated Single-Domain Magnetic Particles Applied to First-Order Reversal Curves

Luca Lanci<sup>1</sup> and Dennis V. Kent<sup>2,3</sup>

<sup>1</sup>Department of Pure and Applied Science, University of Urbino, Urbino, Italy, <sup>2</sup>Department of Earth and Planetary Sciences, Rutgers University, Piscataway, NJ, USA, <sup>3</sup>Lamont-Doherty Earth Observatory of Columbia University, Palisades, NY, USA

**Abstract** Theoretical first-order reversal curves (FORCs) were generated by numerically solving a thermally activated Stoner-Wohlfarth model for assemblages of randomly oriented magnetic particles. The thermally activated Stoner-Wohlfarth model extends previous models based on Preisach theory. The new numerical simulations show that the shapes of reversal curves and the FORC distributions are significantly modified by the effect of the thermal energy only if superparamagnetic particles are predominant. However, most assemblages containing moderate amounts of superparamagnetic particles are hardly distinguishable from stable single-domain assemblages. The most relevant thermal effect is a reduction of coercivity that translates in a shift of the FORC distribution toward the origin. Not all of the distinctive characteristics previously predicted for superparamagnetic grain assemblages were confirmed by our calculations, and most of the observed modifications due to thermal effects can be considered minor. A direct comparison with hysteresis parameters shows that these simpler experiments can be equally effective in characterizing viscous and superparamagnetic particles.

## 1. Introduction

Stable single-domain (SD) ferromagnetic particles have a rather narrow range of grain size but are considered the ideal and most reliable magnetic phase for paleomagnetic and paleointensity studies. There is a quantitative theoretical background that supports the study of these particles, which can be extended toward smaller superparamagnetic (SP) sizes applying the Néel (1949) theory of thermal relaxation. More generally, noninteracting, ultrafine magnetic particles with grain sizes ranging from the SP to stable SD size are not only important carriers of natural remanent magnetization but have many uses as paleoenvironmental tracers. A precise characterization of ultrafine magnetic particles often is desirable, and FORCs provide a potentially powerful tool to discriminate a range of properties from magnetostatic interaction to domain state (e.g., Egli et al., 2010; Muxworthy et al., 2004; Pike, 2003; Pike et al., 1999; Roberts et al., 2000). FORC diagrams have become commonly employed in a wide range of applications in environmental and rock magnetic studies.

The theoretical aspects of FORC diagrams were initially investigated by Pike et al. (1999), Roberts et al. (2000), Pike et al. (2001), and Pike (2003) based on Preisach theory (Preisach, 1935). A more realistic and complete model based on Stoner-Wohlfarth particles (Stoner & Wohlfarth, 1948) has been elaborated by Newell (2005) and further developed by Egli (2006) that also included a partial theory of thermally activated grains. However, there are several details of FORC diagrams of assemblages of SP to viscous SD particles that remain unclear. Strictly speaking SP particles cannot be detected in FORC diagrams because theoretically they have no remanence. What we are aiming at are the fine-grained magnetic particles that are not in thermal equilibrium at room temperature and typical laboratory measurement times; hence, they exhibit an unstable remanence that affects the FORC distribution and more generally the hysteresis loops. The dimensions of these SP particles can range in diameter from a few nanometers to the threshold stable SD range of around 50 nm for magnetite.

FORC diagrams of SP particles were first described by Roberts et al. (2000) and Pike et al. (2001). They distinguished four distinctive traits that characterize the presence of these particles: (1) a shift of the FORC distribution to lower coercivities, (2) the presence of a secondary peak about the origin in the horizontal ridge in addition to the primary stable SD peak, (3) a systematic upward shift of the FORC distribution, and (4) the presence of positive contours that lie near and parallel to the vertical axis in the lower quadrant of a FORC diagram.

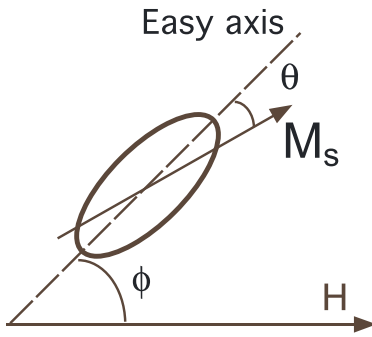


Figure 1. Geometrical elements of a Stoner-Wohlfarth particle.

The theory outlined in Pike et al. (2001), which is based on Preisach theory and a relaxation model strictly valid only at  $H = 0$ , gave us the motivation to investigate theoretical behavior of SP particles in FORC diagrams using a more complete numerical model based on thermally activated Stoner-Wohlfarth particles. We computed FORCs of noninteracting particles at room temperature (300 K) with variable volumes chosen to range in behavior from stable SD to SP and compared the characteristics of the FORC distributions with those of equivalent hysteresis loops. To illustrate several possible situations, we have considered different assemblages of randomly oriented Stoner-Wohlfarth particles, from very simple assemblages with single volume and single coercivity to more realistic ones with distributed volumes and coercivities. Furthermore, we investigate the effect of field step resolution and time interval on the FORC distribution.

## 2. Model's Theory

The numerical model we used for the FORC calculations is derived from that applied to simple hysteresis loops by Lanci and Kent (2003). As in the previous study we consider the classic Stoner-Wohlfarth model of noninteracting, SD particles, with uniaxial anisotropy where the switch of the magnetic moment occurs by coherent rotation. The theory behind the numerical calculations is described below. The actual calculations were performed using a computer program written in C language (Kernighan B. W. & Ritchie, 1988). Random distributions needed in the simulations were generated using the Gnu Scientific Library (Galassi et al., 2009), and the roots of the quartic polynomial (equation (4)) were computed using the C translation of the well-known and tested NETLIB routine RPOLY.FOR.

Compared to the Lanci and Kent (2003) method, calculation speed and numerical precision have been improved by the new solution of equation (2). As easily understood, the numerical errors are not uniform with respect to  $H$  and are also weakly dependent on the number of particles used in the simulation. In our case the error of normalized magnetization, estimated for the whole range of  $H$ , is about  $\sigma \approx 5 \times 10^{-4}$ , which is at least an order of magnitude better than typical laboratory measurements. The numerical precision of our data can be also appreciated by inspection of the computed data included in the supporting information.

### 2.1. The Stoner-Wohlfarth Model

The free energy  $E(\theta)$  of a single magnetic particle is expressed by the sum of the anisotropy and magnetostatic terms (e.g., Bertotti, 1998, and references therein)

$$E(\theta) = v (K_u \sin^2 \theta - \mu_0 H M_s \cos(\phi - \theta)) \quad (1)$$

where  $v$  is the particle volume,  $K_u$  the anisotropy constant,  $M_s$  its spontaneous magnetization, and  $H$  the magnetic field. The angle  $\phi$  is the orientation of the particle's "easy axis" with respect to the direction of  $H$ , and  $\theta$  is the angle between the easy axis and the magnetic moment of the particle (Figure 1).

The stable states of the particle's magnetic moment (i.e., its direction  $\theta$ ) correspond to the minima of the free energy function  $E(\theta)$ . Stable  $\theta$  correspond, therefore, to  $\frac{\partial E}{\partial \theta} = 0$  and  $\frac{\partial^2 E}{\partial \theta^2} > 0$ . The first derivative of  $E(\theta)$

$$\frac{\partial E}{\partial \theta} = v (K_u \sin 2\theta - \mu_0 M_s H \sin(\phi - \theta)) = 0 \quad (2)$$

has, in general, four solutions that represent minima and maxima of  $E(\theta)$ . All solutions are of interest since we need  $\theta$  corresponding to energy minima (i.e., stable states) as well as the energy values of minima and maxima, which are used to compute the energy barriers. We have used the following solution of (2).

$$\theta_{1...4} = \arctan\left(\frac{A}{B}\right) \quad (3)$$

where

$$B = -\frac{A H \mu_0 M_s \cos(\phi)}{2A K_u - H \mu_0 M_s \sin(\phi)}$$

and  $A$  are the roots of the fourth-order polynomial

$$ax^4 + bx^3 + cx^2 + dx + e \quad (4)$$

with the following coefficients:

$$\begin{aligned} a &= 4K_u^2 \\ b &= -4K_u H \mu_0 M_s \sin(\phi) \\ c &= H^2 \mu_0^2 M_s^2 - 4K_u^2 \\ d &= 4K_u H \mu_0 M_s \sin(\phi) \\ e &= -H^2 \mu_0^2 M_s^2 \sin^2(\phi). \end{aligned}$$

Minima and maxima were distinguished by sorting the corresponding values of  $E(\theta)$ .

## 2.2. Néel's Relaxation

The thermodynamical effect was modeled according to Néel's theory (Néel, 1949, 1955). This model assumes that the magnetic moment of a particle can occupy only the two states corresponding to  $E(\theta)$  minima with the magnetic moment switching between the two energy wells. For such a *bi-state* particle the probability of the magnetization being in a given state is described by the so-called kinetic equation (e.g., Bertotti, 1998, and references therein):

$$\frac{dn_1}{dt} = -n_1 w_1 + n_2 w_2 \quad (5)$$

where  $n_{1,2}(t, K_u, v, H, T, \phi)$  is the probability of the moment being in states 1 and 2, respectively ( $n_1 + n_2 = 1$ ) and  $w_{1,2} = f_0 \exp(-Eb_{1,2}/k_b T)$ , with  $Eb_{1,2}$  indicating the blocking energy and  $k_b$  the Boltzmann constant. The preexponential factor  $f_0$  represents the atomic reorganization frequency, which is a function of  $K_u, M_s, T, H$ , and  $\phi$ . Several formulations are reported in the literature (e.g., Brown, 1963); here we consider  $f_0 \simeq 1 \times 10^9$  Hz, as suggested by Moskowitz et al. (1997), and constant, arguing that the exponential terms dominate the variability.

The  $n_1 w_1$  and  $n_2 w_2$  terms in (5) describe the probability of the magnetic moment to switch from state 1  $\rightarrow$  2 and from 2  $\rightarrow$  1, respectively, according to Arrhenius statistics. After substituting  $n_2 = 1 - n_1$  and integrating (5) with respect to  $t$  (assuming thus  $T$  and  $Eb_{1,2}$  constant in  $t$ ), we obtain the classic expression of the approach to thermal equilibrium, for example (Bertotti, 1998),

$$n_1(t) = n_{\text{eq}} + (n_1(0) - n_{\text{eq}}) \exp\left(-\frac{t}{\tau}\right) \quad (6)$$

where

$$n_{\text{eq}} = \frac{w_2}{w_1 + w_2}; \text{ and } \frac{1}{\tau} = w_1 + w_2.$$

The term  $n_{\text{eq}}$  represents the magnetization at the thermodynamical equilibrium, while  $n_1(0)$  is the initial fraction of moments in state 1. In FORC calculations the initial state at the beginning of each reversal curve is inherited from saturation, hence is  $n_1 = 1$ . Notice that the classic Néel relaxation time  $\tau = f_0^{-1} \exp\left(\frac{v h_c M_s}{2 k_b T}\right)$  is a particular case of (6) for an axially symmetric free energy function (i.e.,  $Eb_1 = Eb_2$ ); hence, this simplified expression is inappropriate to compute the relaxation for  $H \neq 0$  as done in Pike et al. (2001).

Since  $\tau$  depends on the energy barriers  $Eb_{1,2}$ , thermal activation introduces a volume dependency into the magnetization model. From (6) the fractions  $n_1(t)$  and  $n_2(t) = 1 - n_1(t)$  can be calculated as a function of time  $t$  and the net magnetization of the ensemble of particles computed by the vector sum of the moments in the two states.

Equation (6) is strictly correct if  $Eb_{1,2}(t)$ , hence,  $H(t)$  is constant; a more rigorous solution for variable  $H(t)$  would require solving the Fokker-Planck equation (Brown, 1963). However, during hysteresis measurements  $H$  is increased in small steps and remains constant during the measurement time of each step. Therefore, we suggest that (6) can still be used appropriately; the thermal effect on the magnetization in this case

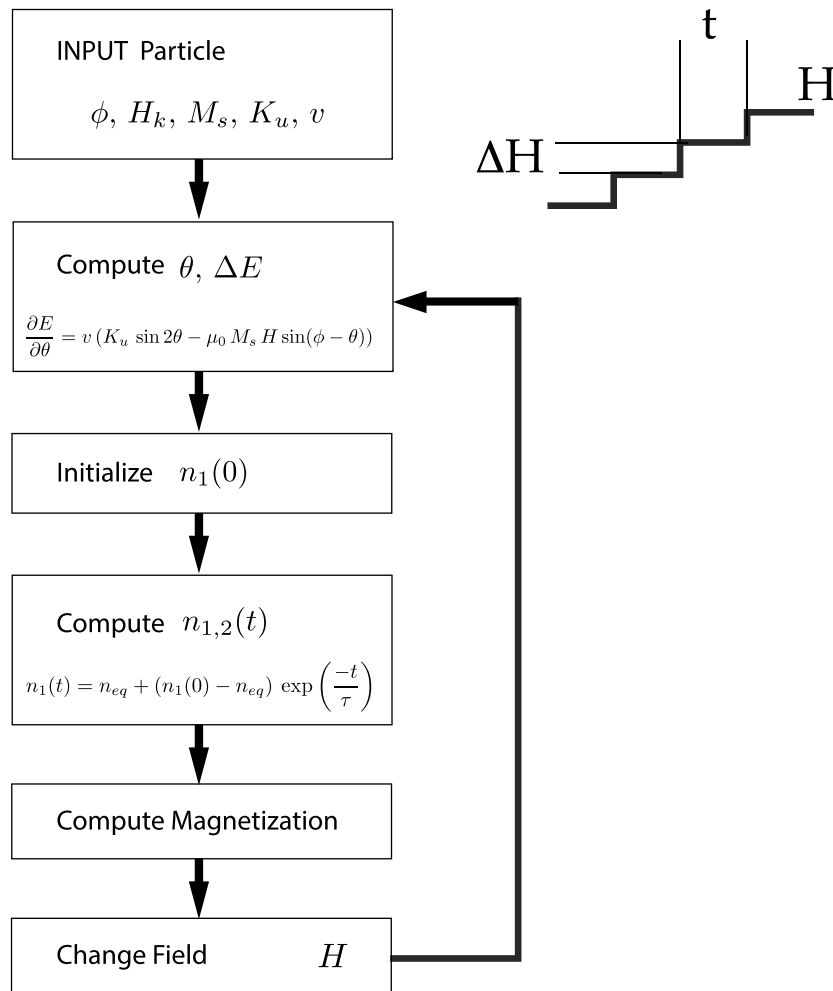


**Figure 2.** Flow diagram for calculations of thermal relaxation using short steps of duration  $t$  with constant  $H$ ;  $\Delta H$  represents the field step.

is computed by numerically integrating (6) at constant  $H$  steps as outlined in Figure 2. Once the probabilities  $n_{1,2}$  and the angles  $\theta_{1,2}$  are computed the particle magnetization  $m$  is computed as

$$m = M_s(n_1 \cos \theta_1 + n_2 \cos \theta_2).$$

### 2.3. Model's Limitation

The most important simplification underlying Néel's relaxation model is based on the separation between switching and nonswitching processes. Moment switching is assumed to occur between two equilibrium configurations corresponding to the minima of the self-energy function equation (1), and within these minima the moment is not perturbed by thermal fluctuations. This is strictly true only at  $T = 0\text{K}$ , since in a real system at  $T > 0$ , the magnetic moment is continuously perturbed, giving rise to significant effects when the thermal energy  $k_B T$  becomes comparable to the energy barrier of the particle. Theoretical calculations (García-Palacios, 2000) have shown that this effect can noticeably decrease the magnetization, compared to Néel's bi-state model, for  $(K_u v)/(k_B T) < 5$ , but the effect declines quickly with increasing  $(K_u v)/(k_B T)$ . To minimize this bias, we restrict our model to  $(K_u v)/(k_B T) \geq 10$ , at room temperature (300 K): for typical magnetite particles this corresponds to a minimum volume of about  $1 \times 10^{-18} \text{cm}^3$  (or an equivalent spherical diameter of about 6 nm). Particles less than this size, which in our computation are completely SP, are probably small enough to be subject to the effects of quantum mechanics and must be treated accordingly. The practical effect of any remaining bias will be a slight overestimate of the intensity of magnetization, but no bias is expected in the calculation of coercivity.

On the opposite side of the modeled grain size spectrum the assumption of coherent rotations limits the maximum grain size of the particles. For magnetite this limit is set between 70 and 100 nm on the basis of micromagnetic calculations (e.g., Dunlop & Özdemir, 1997; Winkelhofer et al., 1997, and references therein); above this size the switch of the particle's magnetic moment occurs with more energetically favorable configurations than coherent rotations (e.g., vortex structures) and they do not behave like Stoner-Wohlfarth particles (e.g., Nagy et al., 2017; Shinjo et al., 2000).

As our model does not consider magnetostatic interaction, this complication is taken out of the simulations allowing us to concentrate on the effect of volume variations. Our results, however, can be easily extended to weakly interacting particles, which includes most natural samples where the concentration of ferromagnetic particles is typically low.

### 3. Model Results

We have performed several numerical simulations using the above model and reproduced simple and more complex situations. In all our simulations the field is switched instantaneously from one intensity value to the next. This is relevant especially for the switch between the saturation field and the beginning of each FORC because the sample is not allowed to relax during this step. This ideal situation is not met in real measurements where there is always some unwanted relaxation during the time needed to ramp the field from the saturating field to the reversal field at the start of each FORC, which attenuates the effect of SP particles on FORC distributions.

The FORC distributions were computed from the raw reversal curves using the FORCinel program (Harrison & Feinberg, 2008). The calculation of a FORC distribution from the raw FORC data is not a trivial process and might shadow features or introduce small artifacts. Thanks to the precision of computed data, we could keep this process as simple as possible using the minimum possible smoothing. Moreover, we provide the raw FORC data in the supporting information. In addition to the FORC distributions, we have computed standard hysteresis parameters (Day et al., 1977) from the FORCs ( $H_{cr}$ ) and from actual hysteresis loops.

#### 3.1. Model With No Thermal Fluctuations

We started from the simplest situation consisting of an assemblage of randomly oriented Stoner-Wohlfarth particles without any thermal perturbation ( $T = 0$  K). This experiment has a solid theoretical background based on Stoner-Wohlfarth theory that can validate numerical results. We computed 400 FORCs from an assemblage of 5,000 noninteracting and randomly oriented grains with field steps  $\Delta H = 1$  mT. It is important to notice that the resolution that we used in these simulations is much higher than typical laboratory measurements, and, as we will discuss later, this can have a significant effect on the FORC distributions. However, high resolution is important to highlight the characteristic of SP particles. We utilized grain parameters typical of magnetite, even though the model is not limited to this ferromagnetic mineral. We used a saturation magnetization  $M_s = 4.8 \times 10^5$  A/m and anisotropy constant  $K_u = 3.0 \times 10^4$  J/m<sup>3</sup> (corresponding to a microscopic coercive force  $H_k = 2K_u/\mu_0 M_s = 9.95 \times 10^4$  A/m or 125 mT) for simulation a0, and a lognormally distributed  $K_u$  with the same mean and  $\sigma = 0.2$  in simulation b0. The intensity of magnetization was normalized to unity in this and all subsequent calculations.

Results of these calculations are shown in Figure 3. Overall, the FORC distribution is virtually identical to that predicted by the theoretical model (Newell, 2005) and numerical calculation of Harrison and Lascau (2014). In agreement with expectations, the main coercivity peak corresponds to  $H_k/2$  in simulation a0. The model is also able to reproduce accurately the predicted negative values in the lower-left area of the FORC diagram near the vertical axis that in Preisach models were erroneously considered a diagnostic feature of interaction (Pike et al., 1999; Stancu et al., 2003). Hysteresis parameters of a0 are those expected for stable SD particles (Table 1), supporting the robustness of the numerical calculations.

#### 3.2. Simple Model With Thermal Fluctuations

More interesting models are obtained when thermal fluctuations became significant in such a simple grain assemblage. These were computed repeating the above FORC simulation a0, using identical parameters at room temperature  $T = 300$  K, but with particles of decreasing volume to test its effect on thermal relaxation. The time elapsed during each magnetization step at constant field is set to  $t = 0.1$  s in this and subsequent calculations. This time constant was chosen to resemble that of real measurements with an alternating gradient field magnetometer, but we will also discuss the effect of  $t$  on the FORC distribution. It might be worth

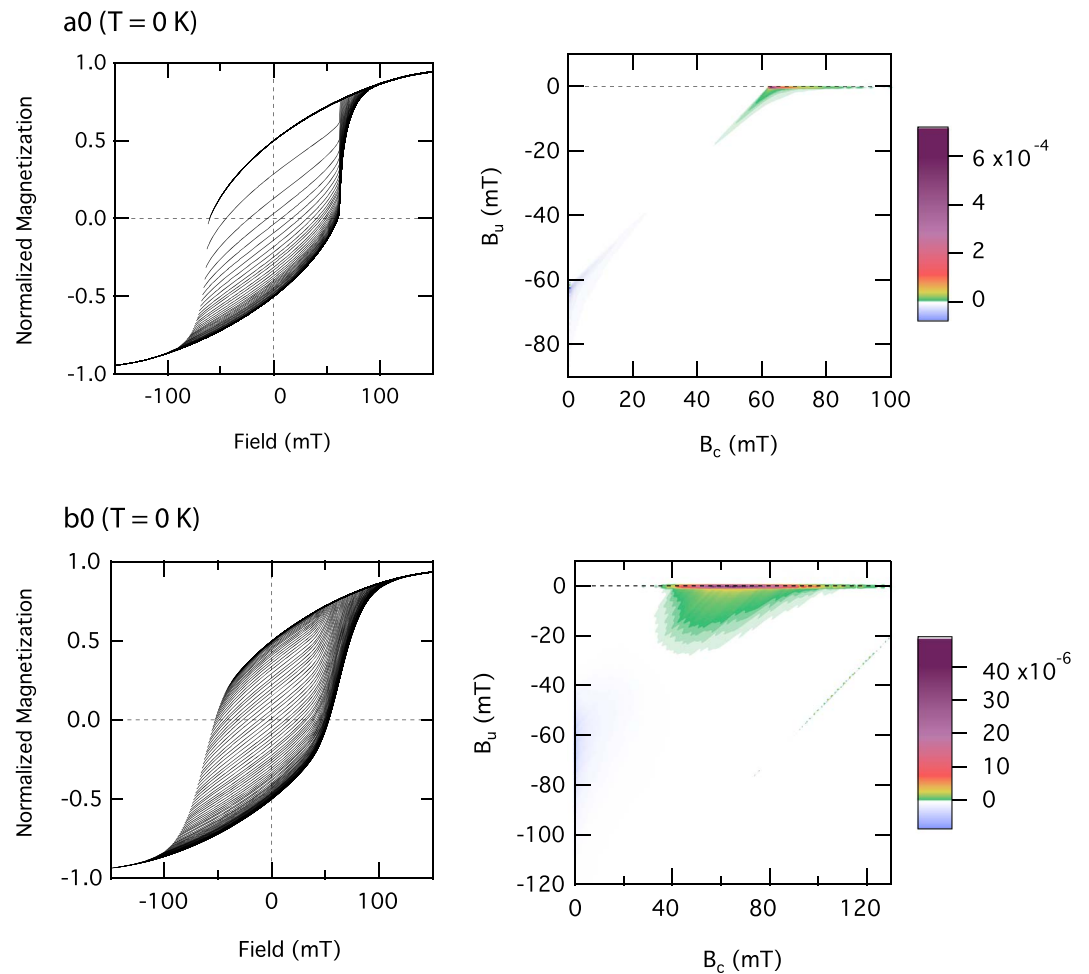


**Figure 3.** Reversal curves and FORC distribution of a randomly oriented assemblage of 5,000 stable single-domain particles. a0 represents a single coercivity assemblage with  $K_u = 3.0 \times 10^4$  J/m and b0 the same assemblage with lognormally distributed  $K_u$ . Hysteresis parameters are reported in Table 1. Other parameters used in calculations are  $\Delta H = 1$  mT and  $M_s = 4.8 \times 10^5$  A/m.

noticing at this point that  $K_u$  influences the blocking energies just like the particle's volume, and the relaxation model could be described as a function of their product. We preferred to keep the two variables separated because it does not add any complications to the simulations. Moreover, in typical magnetite samples the variability of  $K_u$  (hence  $H_k$ ) has a limited range compared to that of volume and in some cases it could be considered a second order variable.

The FORC distributions of these assemblages are shown in Figure 4. Grain volumes of  $1 \times 10^{-16}$ ,  $1 \times 10^{-17}$ ,  $5 \times 10^{-18}$ , and  $4 \times 10^{-18}$  cm<sup>3</sup>, from a1 to a4, respectively, were chosen to range from nearly stable SD to strongly SP. The FORC distribution of simulation a1, with the largest volume  $v = 1 \times 10^{-16}$  cm<sup>3</sup>, is almost identical to a0 and apparently does not show any sign of relaxation. However, some relaxation does in fact occur and can be noticed by the shift toward the origin of the main ridge compared to the expected value of  $H_k/2$ . The main differences between this and the progressively more SP assemblages a2, a3, and a4 are even more pronounced shifts of the main peak toward the origin, its spread along the vertical axis as theoretically predicted by Egli (2006), and the development of the positive ridge along the vertical axis according to the prediction of Egli (2006) and Pike et al. (2001). These effects start to become evident for particle volumes smaller than approximately  $1 \times 10^{-17}$  cm<sup>3</sup> (a2) and increase quickly with small volume variations. The fine positive ridge near the vertical axis of the FORC distribution results from a strong relaxation of the SP particles at the beginning of the FORC that produces observable concave magnetization curve. The negative well disappears in a4 and all the values of the FORC distribution become positive. Other minor changes include the shape of the main peak that gradually loses the higher coercivity "tail" and the "boomerang" shape typical of stable SD.

**Table 1**  
Hysteresis Parameters

Assemblage	$M_s$	$M_{sr}$	$H_{Cr}$ (mT)	$H_c$ (mT)	$H_{Cr}/H_c$
a0 ( $T = 0K$ )	1	0.5	65.5	60.3	1.09
a1	1	0.5	60.1	57.2	1.05
a2	1	0.5	39.9	38.6	1.02
a3	1	0.5	24.5	24.3	1.01
a4	1	0.5	18.0	16.4	1.09
b0 ( $T = 0K$ )	1	0.5	68.5	53.1	1.29
b1	1	0.5	62.8	50.3	1.25
b2	1	0.5	41.5	35.2	1.18
b3	1	0.5	24.9	21.5	1.16
b4	1	0.49	18.1	15.2	1.19
b5	1	0.38	10.9	5.68	1.92
b6	1	0.05	6.05	0.29	20.8
c1	1	0.47	35.3	26.5	1.33
c2	1	0.36	19.4	10.3	1.88

It is worth noticing that the hysteresis parameters of these assemblages show a decrease of coercivity  $H_c$  that correlates with the shift of the central ridge, but despite the significant thermal relaxation effect, there is no change in  $M_{sr}$  (Table 1) and the hysteresis parameters are practically indistinguishable from that of stable SD.

### 3.3. Model With Distributed $K_u$

Models of assemblages of grains with single-valued  $v$  and  $K_u$  serve as useful simplified examples but are not very realistic. FORC distributions more similar to natural samples can be obtained using grain assemblages with distributed  $K_u$ . Following Robertson and France (1994), we use a lognormal distribution of  $K_u$  with  $\mu = 3.0 \times 10^4 \text{ J/m}^3 \text{ mT}$  and  $\sigma = 0.2$  and keep the grain volumes single valued to better analyze the volume dependence of the FORC diagram. This ties up the  $K_u$  with the  $Eb$  distributions that are simply proportional; all other parameters are the same as the previous simulations.

As in the previous case, the FORCs were computed for grain assemblages of decreasing volumes  $v = 1 \times 10^{-16}$ ,  $1 \times 10^{-17}$ ,  $5.0 \times 10^{-18}$ ,  $4.0 \times 10^{-18}$ ,  $3.0 \times 10^{-18}$ ,  $2.0 \times 10^{-18} \text{ cm}^3$  from b1 to b6, respectively, and are shown in Figure 5.

Simulation b1 reproduces closely the FORC distribution of the stable SD example b0 with no apparent indications of relaxation. However, just like a1 the reduced coercivity  $H_c$  compared to simulation b0 indicates the presence of a small influence of thermal fluctuations (Table 1). With decreasing volume, hence increasing thermal perturbation, we notice again an increased shift of the central ridge toward the origin of the FORC diagram, the increase of its thickness, and the progressive development of the positive ridge near the vertical axis. These occur without the development of other peculiar characteristics until the assemblage became strongly SP and the main peak gets very close to the origin. In assemblages b5 and b6 ( $v = 3.0 \times 10^{-18} \text{ cm}^3$  and  $v = 2.0 \times 10^{-18} \text{ cm}^3$ ), the FORC distribution has only positive values and the main horizontal ridge merges with the vertical ridge at  $H_c \approx 0$ . This provides a numerical analog to the data reported, for instance, in sample CS914 from the Yucca Mountain Tuff by Roberts et al. (2000) and Pike et al. (2001).

As in simulations a1–a4, the gradual shift of the central ridge in the FORC distribution is paralleled by the progressive thinning of hysteresis loops and reduced coercivity  $H_c$  (Table 1). The hysteresis parameters of b1–b3 do not significantly differ from that of stable SD, but interestingly, the hysteresis parameters of b5 and b6, which are still larger than the smallest volume that we consider admissible in our model, are clearly different from that of other simulations.

### 3.4. Model With Distributed $K_u$ and Volume

As a further step toward more realistic situations, we compute FORC diagrams of ensembles with particles ranging from SP to stable SD. These ensembles have distributed  $K_u$  and volume  $v$ , hence a distribution of  $Eb = K_u v$ . Lacking experimental data on the volume distribution of magnetic particles in natural samples,

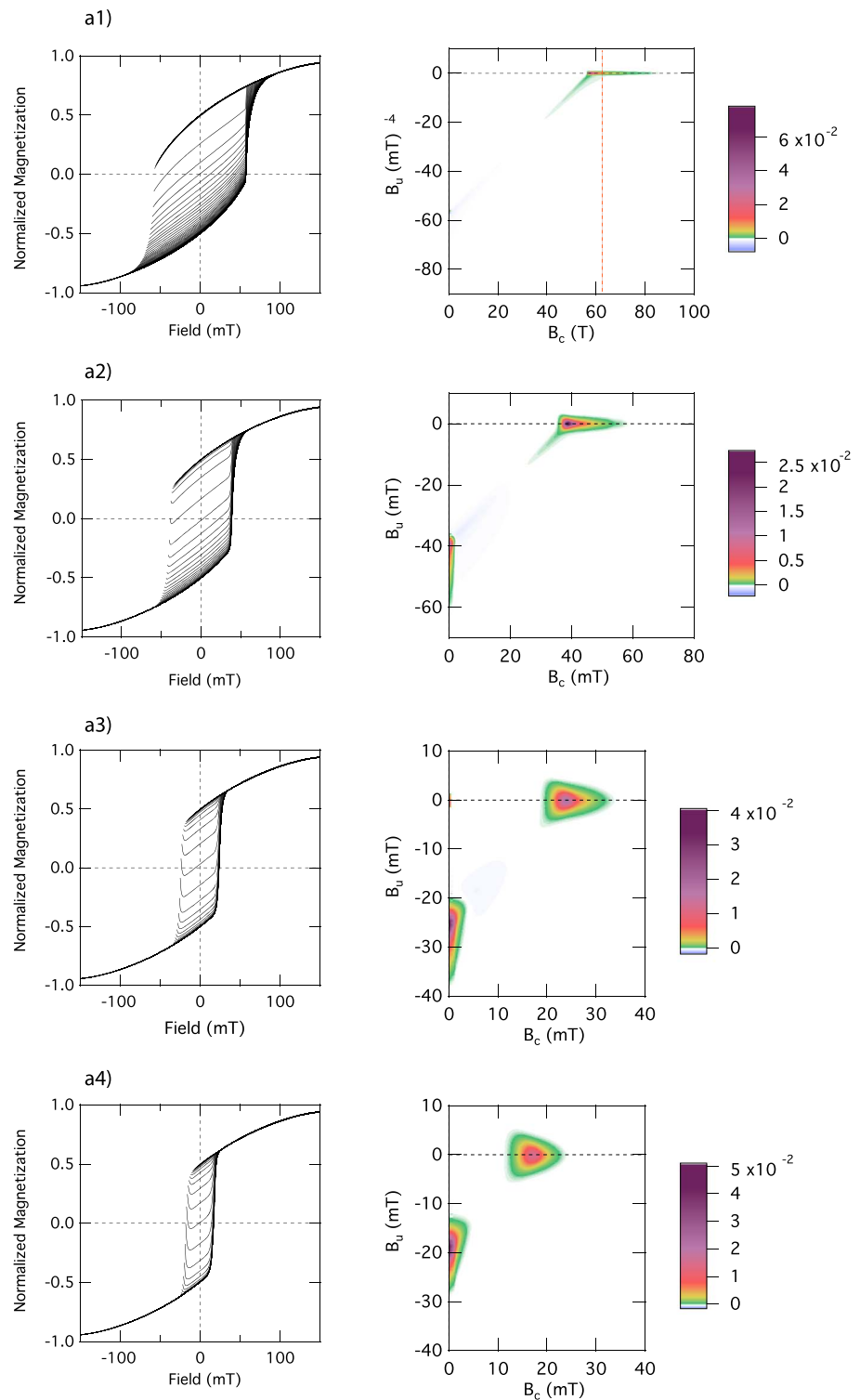


**Figure 4.** Reversal curves and first-order reversal curve distributions computed from 400 reversal curves of an assemblage of 5,000, thermally activated, randomly orientated particles of decreasing volumes  $v = 1 \times 10^{-16}$ ,  $1 \times 10^{-17}$ ,  $5 \times 10^{-18}$ , and  $4 \times 10^{-18}$  cm<sup>3</sup> from a1) to a4), respectively. The red dashed line in a1) represents the  $H_k/2$  value (the expected position of the peak of the horizontal ridge in a stable single-domain assemblage). The shift toward the origin indicates relaxation despite the lack of other features. Other parameters used in calculations are  $\Delta H = 1$  mT,  $T = 300$  K,  $t = 0.1$  s,  $K_u = 3.0 \times 10^4$  J/m, and  $M_s = 4.8 \times 10^5$  A/m. Raw first-order reversal curve data are provided in supporting information.

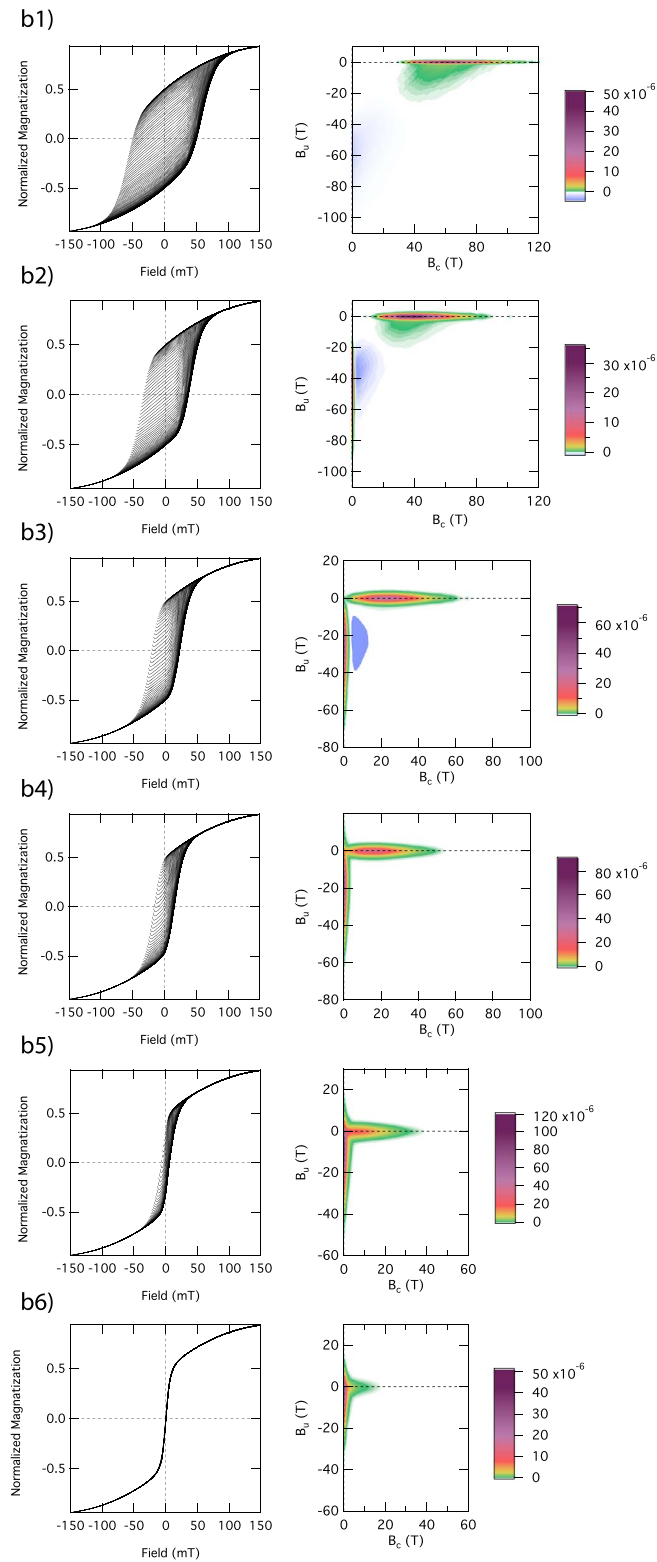


**Figure 5.** Reversal curves and first-order reversal curve distributions of thermally activated assemblages of randomly orientated particles with lognormal-distributed  $K_u$  ( $\mu = 3.0 \times 10^4$  J/m and  $\sigma = 0.2$ ) and decreasing volumes of  $1 \times 10^{-16}$ ,  $1 \times 10^{-17}$ ,  $5.0 \times 10^{-18}$ ,  $4.0 \times 10^{-18}$ ,  $3.0 \times 10^{-18}$ , and  $2.0 \times 10^{-18}$  cm<sup>3</sup>, from b1 to b6, respectively. The thermal relaxation affects all the assemblages and increases with decreasing volumes. Other parameters used in calculations are  $\Delta H = 1$  mT,  $T = 300$  K,  $t = 0.1$  s, and  $M_s = 4.8 \times 10^5$  A/m. Raw first-order reversal curve data are provided in the supporting information.

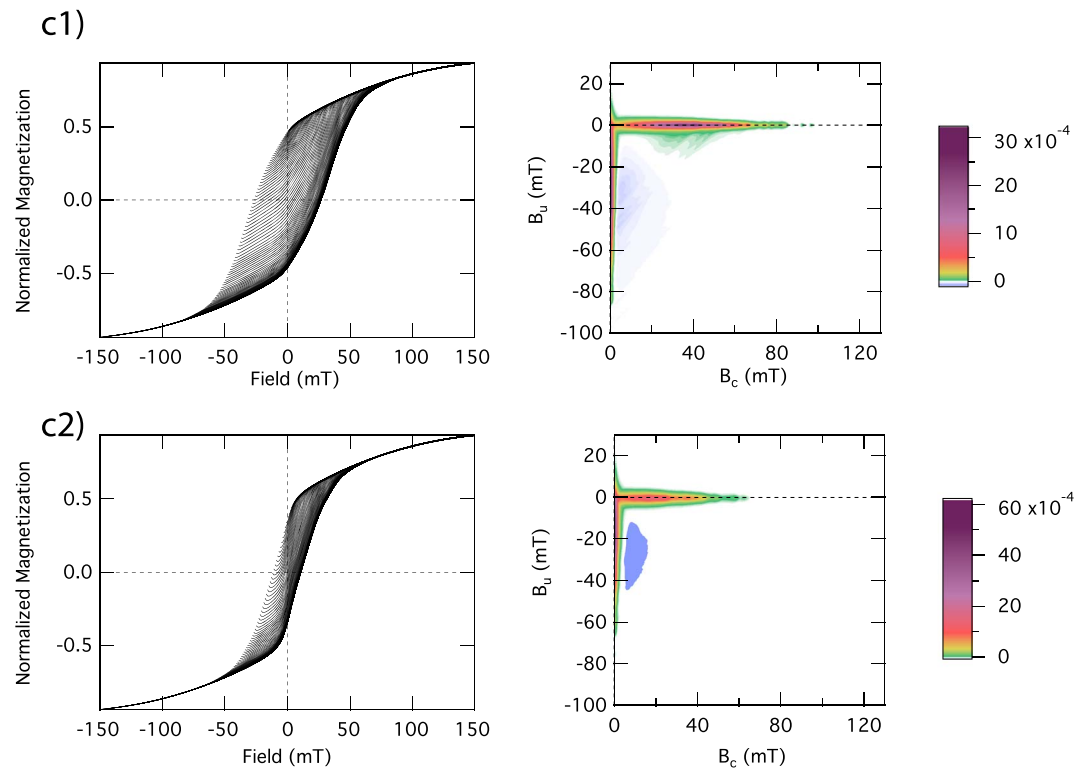


**Figure 6.** Reversal curves and first-order reversal curve distributions of thermally activated assemblages of randomly orientated particles with log-normal distributed  $K_u$  ( $\mu = 3.0 \times 10^4$  J/m and  $\sigma = 0.2$ ) and volumes ( $\mu = 5 \times 10^{-18}$  cm<sup>3</sup> and  $\sigma = 0.6$  in c1 and  $\mu = 3 \times 10^{-18}$  cm<sup>3</sup> and  $\sigma = 0.4$  in c2). Other parameters used in calculations are  $\Delta H = 1$  mT,  $T = 300$  K,  $t = 0.1$  s, and  $M_s = 4.8 \times 10^5$  A/m. Raw first-order reversal curve data are provided in the supporting information.

we have used a lognormal distribution also for particle volumes since this seems a natural distribution for nonnegative values and is often used in granulometric analysis.

Simulation c1 (Figure 6) shows the FORC diagram of a sample with the same characteristics of simulation b3 but with a lognormally distributed volume of grains with  $\mu = 5 \times 10^{-18}$  cm<sup>3</sup> and  $\sigma = 0.6$ , corresponding to grain volumes ranging from approximately  $1.5 \times 10^{-18}$  to  $4.8 \times 10^{-17}$  cm<sup>3</sup>, and equivalent spherical diameter from approximately 7.1 to 22 nm. Nearly all the grains in this assemblage are in the SP range at  $T = 300$  K. The positive ridge near the vertical axis at  $H_c \approx 0$  is well developed in both assemblages, but negative values are still found. The crossing of the main horizontal ridge and the vertical ridge produces a sharp increase of the FORC distribution at the origin. It would not be unreasonable to interpret this feature as the secondary peak described by Roberts et al. (2000) and Pike et al. (2001) even though they have observed it in the absence of the vertical ridge.

All these characteristics are emphasized in simulation c2, which uses a lognormal volume distribution with  $\mu = 3 \times 10^{-18}$  cm<sup>3</sup> and  $\sigma = 0.4$ , corresponding to grains volume ranging from approximately  $1.0 \times 10^{-18}$  to  $1.3 \times 10^{-17}$  cm<sup>3</sup>.

The presence of SP particles can be appreciated as well from the hysteresis parameters. Although hysteresis parameters of c1 are only slightly different from those of stable SD and similar to those of simulation b4, the abundant presence of SP particles in c2 gives noticeably different parameters that have values similar to b5 (Table 1).

### 3.5. Influence of Measurement Parameters

The field step resolution ( $\Delta H$ ) used in our simulations is much higher than typical laboratory measurements, and the simulations shown above would not be easily reproduced in actual laboratory measurements; moreover, the time step  $t$  can change considerably in real measurements. We have therefore investigated whether and to what extent FORCs can be influenced by the parameters  $\Delta H$  and  $t$  by repeating the previous simulations with  $\Delta H \sim 4$  mT, which is typical of good quality laboratory measurements, and different  $t$ .

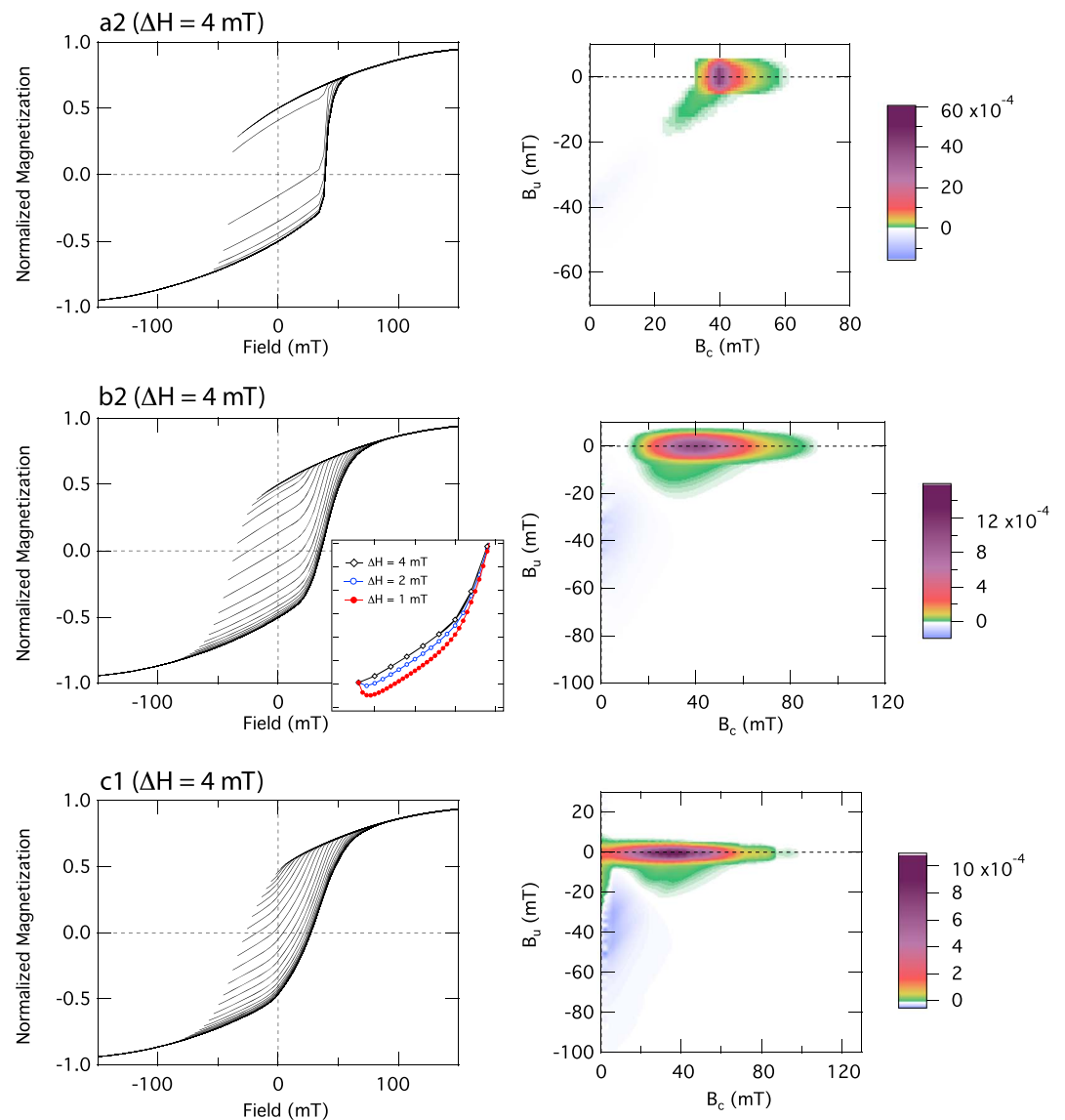


**Figure 7.** Effect of field step  $\Delta H$  on first-order reversal curve (FORC) of thermally activated assemblages of randomly orientated particles. Except for the larger field step  $\Delta H = 4$  mT, the simulation parameters are the same for a2 (Figure 4), b2 (Figure 5), and c1 (Figure 6). In these simulations, as a result of the larger  $\Delta H$ , the concavity at the beginning of each FORC is missing and consequently the positive ridge near the vertical axis of the FORC distribution is absent or very attenuated. In the insert of b2 an example of a single reversal curve that shows the different paths of the magnetization as a result of different  $\Delta H$  is shown.

The outcome is somewhat surprising: the larger  $\Delta H$  does not only affect the details of the measurements but changes the shape of the reversal curves especially in the initial part where the relaxation of SP particles plays a relevant role. This is a consequence of the strong nonlinear dependence of relaxation from the energy barriers, hence ultimately from  $H$ , that results in a different path of the magnetization curve. Explicative examples of FORC distributions computed with the field step  $\Delta H \sim 4$  mT are shown in Figure 7 and can be compared with high-resolution calculations in a2 (Figure 4), b2 (Figure 5), and c1 (Figure 6). Some characterizing features visible in high-resolution simulations, such as vertical ridge near the vertical and the thickening of the main ridge, are attenuated or hidden in these lower-resolution examples. Comparing the reversal curves with the corresponding high-resolution reversal curves (inset for b2 in Figure 7), one notices that bigger field steps result in a much larger relaxation during the initial steps that reduces or conceals the concave shape at the beginning of the FORC, typical of SP assemblages.

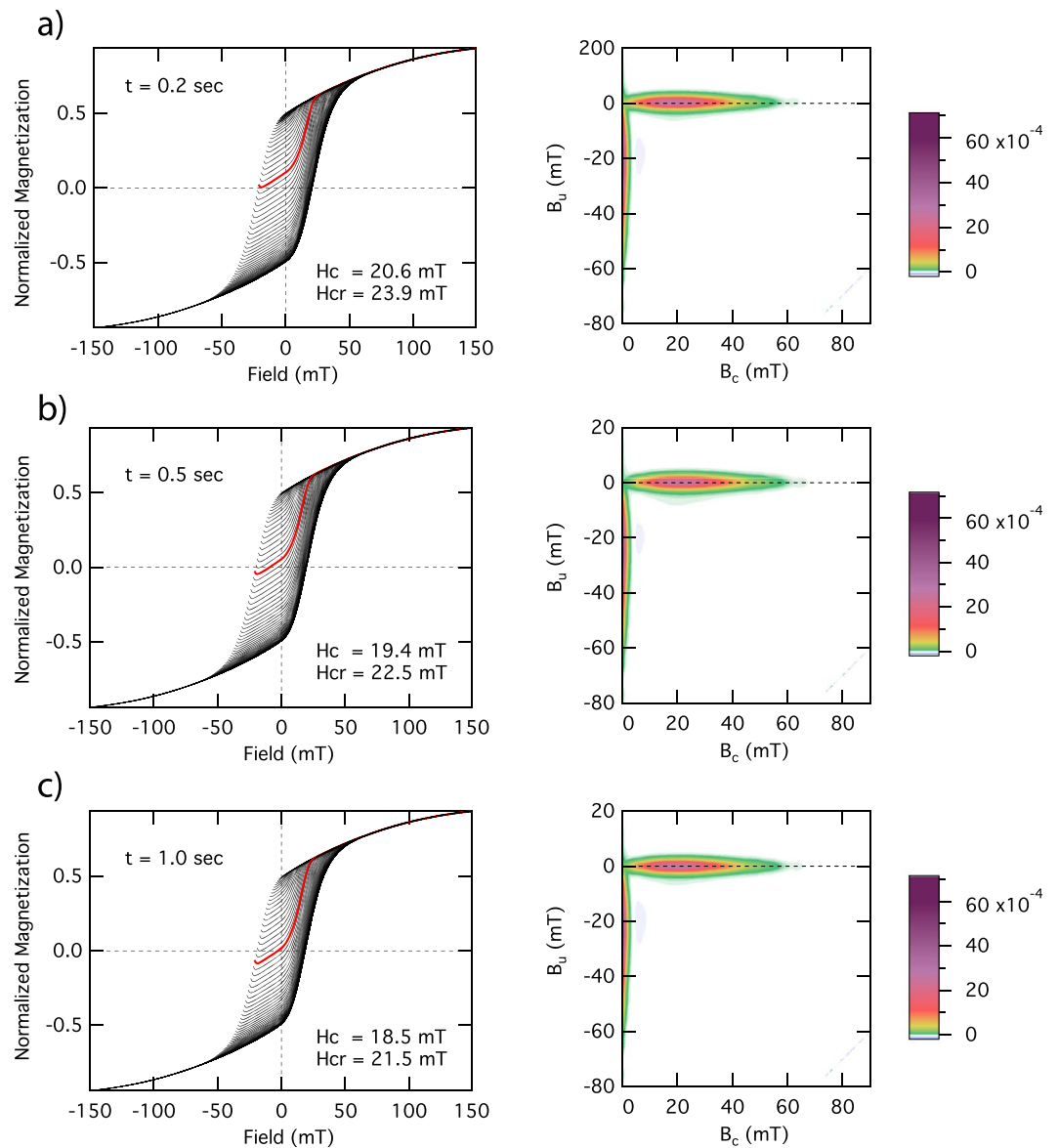


**Figure 8.** Effect of different time  $t$  on first-order reversal curve of a thermally activated assemblages of randomly orientated particles. Simulation parameters are the same of b3 (Figure 5) with time steps of  $t = 0.2$  s,  $t = 0.5$  s, and  $t = 1$  s in panels (a)–(c), respectively. The effect of  $t$  on the first-order reversal curve distribution is minimal and hard to notice; it can be better seen in the actual reversal curves (left panel) as a change of coercivity  $H_c$  and coercivity of remanence  $H_{cr}$ . The same reversal curve ( $H_a = 21$  mT) is marked in red in all simulations to highlight the effect of  $t$ .

On the contrary, we have found that the measurement time  $t$  does not have a strong influence on the shape of the reversal curves, hence, on the FORC distribution. With increased  $t$  the reversal curves decrease their initial magnetization due to the larger relaxation, but the overall shape does not change much, in particular the concave feature in the initial part typical of SP particles is retained. With increasing reversal fields the longer  $t$  increases the probability of the magnetic moment switching due to thermal fluctuations and this results in a lower coercivity of the ensemble. In fact, the most noticeable effect of increasing  $t$  on FORCs are the reduced coercivity  $H_c$  and coercivity of remanence  $H_{cr}$  (Figure 8).

#### 4. Discussion

FORC diagrams of stable SD assemblages obtained from our numerical model are virtually identical to those predicted by the theoretical model based on Stoner-Wohlfarth particles (Egli, 2006; Newell, 2005).

Moreover, they also reproduce all the major characteristic predicted by Egli (2006) for thermally activated Stoner-Wohlfarth particles, testifying to the robustness of the numerical model. Our results extend the thermally activated Stoner-Wohlfarth theory providing many details that are not available from previous treatments.

Thermally activated ensembles suggest that in magnetic particles with parameters typical of magnetite at room temperature and with a rather short measurement time typical of alternating gradient field magnetometers, the effects of thermal fluctuations start in volumes as large as  $1 \times 10^{-17} \text{ cm}^3$  but become evident only for smaller particles. The most notable effect on the FORC distribution consists in a shift of the central ridge, or peak, toward the origin in accordance with the thermally reduced distribution of blocking energy. The corresponding feature in simple hysteresis loops is an equivalent decrease of coercivity  $H_c$  (Figure 5). The shift of the central ridge and decrease of  $H_c$  in simple hysteresis loops are very sensitive to SP particles and relatively insensitive to field step parameter  $\Delta H$ . Unfortunately, this characteristic cannot be easily noticed without knowing the a priori equivalent  $H_c$  for stable SD state.

One peculiar characteristic for SP predicted by Pike et al. (2001) and observed in experimental data from predominantly SP samples such as the Yucca Mountain Tuff is the development of a positive ridge near the vertical axis of the FORC distribution. Our high-resolution simulations have been able to reproduce this feature in great detail, and also to show its origin in the concavity resulting from the strong relaxation at the beginning of each FORC curve. However, the positive (concave) curvatures of the initial part of reversal curves that can be easily observed in the high-resolution data might disappear with larger  $\Delta H$  (Figure 7). On the other hand, the FORC distribution is not particularly sensitive to changes of the measurement time  $t$ , which mostly affects  $H_c$  and  $H_{cr}$ .

The problem of sensitivity to measurement parameters is not specific to FORCs but a more general problem that should suggest prudence in applying such techniques as quantitative tools to evaluate the presence of SP particles. The main consequence on FORC distributions is that the positive ridge near the vertical axis becomes more difficult to observe in simulations in which the field steps are similar to that of typical laboratory measurements (Figure 7), and presumably, the ridge would be even more difficult to observe in real experiments in which the time elapsed between saturation and the first measure is not negligible.

In our models with SP assemblages, the displacement toward the origin of the main ridge is observed together with its widening along the vertical axis predicted by the theory of Egli (2006). The central ridge remains centered along the horizontal axis at  $H_u = 0$ , and the model does not clearly reproduce the secondary peak near the origin similar to that observed in experimental results (Pike et al., 2001; Roberts et al., 2000). However, in some SP assemblages, when the positive crest along the vertical axis is well developed and reaches the origin, it can intersect with the main horizontal ridge and give rise to a well-developed positive peak that can be interpreted as the aforementioned peak. An alternative explanation for the secondary peak observed by Roberts et al. (2000) and Pike et al. (2001) is that it originates from bimodal distributions of  $K_u$  and/or volumes and, therefore, could be considered indicative of such situations.

## 5. Conclusions

We have presented a number of numerical simulations describing situations from the most simple to more realistic that illustrate the theoretical FORC distribution of assemblages of particles from stable SD to SP.

Our new calculations could reproduce faithfully the theoretical properties of stable SD and SP particles predicted by Newell (2005) and Egli (2006), and could confirm two of the four main characteristics of SP particles suggested by Roberts et al. (2000) and Pike et al. (2001), namely, the presence of positive contours along the vertical axis in the lower quadrant and the shift of the main FORC distribution toward the origin.

Furthermore, for SP particles we have found a strong dependence on the FORC from the field step  $\Delta H$ . SP characteristics could be plainly observed only in the high-resolution simulations (field steps  $\Delta H = 1 \text{ mT}$ ), whereas using field steps of  $\Delta H \sim 4 \text{ mT}$ , which are more typical of high-quality laboratory measurements, some of these characteristics are much attenuated. The strong sensitivity to the experimental conditions suggests a certain caution should be exercised in the use of these methods as quantitative tools to characterize SP samples.

The shift of the main ridge toward the origin is a robust characteristic of SP assemblages that is not sensitive to the measurements resolution. However, it is very difficult to distinguish a low coercivity assemblage of stable

SD grains from a high coercivity assemblage of SP grains whose coercivity has been reduced by thermal activation. From this point of view, FORC diagrams, and hysteresis loops in general, are not effective quantitative tools for recognizing the presence of SP particles in natural samples, unless SP particles are predominant and the minor features became observable even at low resolution. In this case, hysteresis parameters seem to be almost equally effective in recognizing the presence of SP particles (Lanci & Kent, 2003).

The strong sensitivity of coercivity to thermal activation combined with the extreme difficulty of recognizing samples whose distribution of coercivity is altered by thermal effects should suggest prudence in the characterization based on the analysis of coercivity of natural samples that potentially contain SP particles.

#### Acknowledgments

We thank R. Harrison and an anonymous reviewer for constructive reviews. Data of reversal curves shown in this paper can be found in the supporting information file. The computer code is available upon request from the corresponding author. This research was partially supported by the University of Urbino and DiSPeA research project 2017. Lamont-Doherty Earth Observatory Contribution 8158.

#### References

- Bertotti, G. (1998). *Hysteresis in magnetism: For physicists, material scientist and engineers*. San Diego, CA: Academic press.
- Brown, W. F. (1963). Thermal fluctuation of a single domain particle. *Physical Review*, *130*, 1677–1686.
- Day, R., Fuller, M., & Schmidt, V. A. (1977). Hysteresis parameters of titanomagnetite: Grain size and compositional dependence. *Physics of the Earth and Planetary Interiors*, *13*, 260–267.
- Dunlop, D. J., & Özdemir, Ö. (1997). *Rock magnetism: Fundamentals and frontiers*. Cambridge: Cambridge University Press.
- Egli, R. (2006). Theoretical aspects of dipolar interactions and their appearance in first-order reversal curves of thermally activated single-domain particles. *Journal of Geophysical Research*, *111*, B12S17. <https://doi.org/10.1029/2006JB004567>
- Egli, R., Chen, A. P., Winklhofer, M., Kodama, K. P., & Horng, C.-S. (2010). Detection of noninteracting single domain particles using first-order reversal curve diagrams. *Geochemistry, Geophysics, Geosystems*, *11*, Q01Z11. <https://doi.org/10.1029/2009GC002916>
- Galassi, M., Davies, J., Theiler, J., Gough, B., Jungman, G., Alken, P., et al. (2009). GNU scientific library reference manual—3rd Ed. Garcia-Palacios, J. (2000). On the statics and dynamics of magneto-anisotropic nanoparticles. *Advances in Chemical Physics*, *112*, 1–210.
- Harrison, R. J., & Feinberg, J. M. (2008). FORCine: An improved algorithm for calculating first-order reversal curve distributions using locally weighted regression smoothing. *Geochemistry, Geophysics, Geosystems*, *9*, Q05016. <https://doi.org/10.1029/2008GC001987>
- Harrison, R. J., & Lascu, I. (2014). FORCulator: A micromagnetic tool for simulating first-order reversal curve diagrams. *Geochemistry, Geophysics, Geosystems*, *15*, 4671–4691. <https://doi.org/10.1002/2014GC005582>
- Kernighan B. W., & Ritchie, D. M. (1988). *The C programming language* (2nd ed.). Englewood Cliffs: Prentice Hall.
- Lanci, L., & Kent, D. V. (2003). Introduction of thermal activation in forward modeling of hysteresis loops for single-domain magnetic particles and implications for the interpretation of the Day diagram. *Journal of Geophysical Research*, *108*(B3), 2142. <https://doi.org/10.1029/2001JB000944>
- Moskowitz, B. M., Frankel, R. B., Walton, S. A., Dickson, D. P. E., Walton, K. K. W., Douglas, T., & Mann, S. (1997). Determination of the pre-exponential frequency factor for superparamagnetic maghemite particles in magnetoferritin. *Journal of Geophysical Research*, *102*(B10), 22,671–22,680.
- Muxworthy, A., Heslop, D., & Williams, W. (2004). Influence of magnetostatic interactions on first-order-reversal-curve (FORC) diagrams: A micromagnetic approach. *Geophysical Journal International*, *158*, 888–897. <https://doi.org/10.1111/j.1365-246X.2004.02358.x>
- Nagy, L., Williams, W., Muxworthy, A. R., Fabian, K., Almeida, T. P., Conbhuí, P. Ó., & Shcherbakov, V. P. (2017). Stability of equidimensional pseudo-single-domain magnetite over billion-year timescales. *Proceedings of the National Academy of Sciences of the United States of America*, *114*(39), 10,356–10,360. <https://doi.org/10.1073/pnas.1708344114>
- Néel, L. (1955). Some theoretical aspect of rock magnetism. *Advances in Physics*, *4*, 191–243.
- Néel, L. (1949). Théorie du trainage magnétique des ferromagnétiques en grains fins avec applications aux terres cuites. *Annales Geophysicae*, *5*, 99–136.
- Newell, A. J. (2005). A high-precision model of first-order reversal curves (FORC) functions for single-domain ferromagnets with uniaxial anisotropy. *Geochemistry, Geophysics, Geosystems*, *6*, Q05010. <https://doi.org/10.1029/2004GC000877>
- Pike, C. R., Roberts, A. P., & Verosub, K. L. (1999). Characterizing interactions in fine magnetic particle systems using first order reversal curves. *Journal of Applied Physics*, *85*(9), 6660–6667.
- Pike, C. R., Roberts, A. P., & Verosub, K. L. (2001). First-order reversal curve diagrams and thermal relaxation effects in magnetic particles. *Geophysical Journal International*, *145*, 721–730.
- Pike, C. R. (2003). First-order 504 reversal-curve diagrams and reversible magnetization. *Physical Review B*, *68*, 104424. <https://doi.org/10.1103/PhysRevB.68.104424>
- Preisach, F. (1935). Über die magnetische Nachwirkung. *Zeitschrift für Physik*, *94*, 277–302.
- Roberts, A. P., Pike, C. R., & Verosub, K. L. (2000). First-order reversal curve diagrams: A new tool for characterizing the magnetic properties of natural samples. *Journal of Geophysical Research*, *105*(B12), 28,461–28,475.
- Robertson, D. J., & France, D. E. (1994). Discrimination of remanence-carrying minerals in mixtures, using isothermal remanent magnetisation acquisition curves. *Physics of the Earth and Planetary Interiors*, *82*, 223–234. [https://doi.org/10.1016/0031-9201\(94\)90074-4](https://doi.org/10.1016/0031-9201(94)90074-4)
- Shinjo, T., Okuno, T., Hassdorf, R., Shigeto, K., & Ono, T. (2000). Magnetic vortex core observation in circular dots of permalloy. *Science*, *289*, 930–932.
- Stancu, A., Pike, C. R., Stoleriu, L., Postolache, P., & Cimpoesu, D. (2003). Micromagnetic and Preisach analysis of the first order reversal curves (FORC) diagram. *Journal of Applied Physics*, *93*(10), 6620–6622.
- Stoner, E. C., & Wohlfarth, E. P. (1948). A mechanism of magnetic hysteresis in heterogeneous alloys. *Philosophical Transactions of the Royal Society, Series A*, *240*, 599–642. reprinted by IEEE Trans. Mag. *27* (4), 3475, 1991.
- Winklhofer, M., Fabian, K., & Heider, F. (1997). Magnetic blocking temperatures of magnetite calculated with a three-dimensional micromagnetic model. *Journal of Geophysical Research*, *102*(B10), 22,695–22,709.